Redispersible Hybrid Nanopowders: Cerium Oxide Nanoparticle Complexes with Phosphonated-PEG Oligomers

Ling Qi,[†] Amit Sehgal,[†] Jean-Christophe Castaing,[†] Jean-Paul Chapel,[†,*] Jérôme Fresnais,[‡] Jean-François Berret,[‡] and Fabrice Cousin[§]

[†]Complex Fluid Laboratory, UMR CNRS/Rhodia 166, CRTB Rhodia Inc., 350 G. Patterson Boulevard, Bristol, Pennsylvania 19007, [‡]Matière et Systèmes Complexes, UMR 7057 CNRS/Université Denis Diderot (Paris 7), Bâtiment Condorcet, 10 rue Alice Domon et Leïonie Duquet, F-75205 Paris, France, and [§]Laboratoire Léon Brillouin, UMR CEA-CNRS 12, CEA- Saclay, 91191 Gif-sur-Yvette, France

ABSTRACT Rare earth cerium oxide (ceria) nanoparticles are stabilized using end-functional phosphonated-PEG oligomers. The complexation process and structure of the resulting hybrid core−shell singlet nanocolloids are described, characterized, and modeled using light and neutron scattering data. The adsorption mechanism is nonstoichiometric, yielding the number of adsorbed chains per particle $N_{ads} = 270$ at saturation. Adsorption isotherms show a high affinity of the phosphonate head for the ceria surface (adsorption energy $\Delta G^{ads} \approx -16kT$) suggesting an electrostatic driving force for the complexation. The *ease*, *efficiency*, and *integrity* of the complexation is highlighted by the formation of nanometric sized cerium oxide particles covered with a well anchored PEG layer, maintaining the characteristics of the original sol. This solvating brushlike layer is sufficient to solubilize the particles and greatly expand the stability range of the original sol (<pH 3) up to pH = 9. We underscore two key attributes of the tailored sol: (i) strong *UV absorption* capability after functionalization and (ii) ability to *redisperse* after freeze-drying as powder in *aqueous or organic solvents* in varying concentrations as singlet nanocolloids. This *robust* platform enables translation of intrinsic properties of mineral oxide nanoparticles to critical end use.

KEYWORDS: nanoparticle · nanopowder · cerium oxide · PEG · phosphonate · adsorption · nonstoichiometric · redispersible

The size-dependent properties of nanoparticles have generated diverse scientific interests. Their high surface area, shape, surface chemistry, and intrinsic properties (dielectric constant, radiation absorption, sensitivity to external field, ...) are currently fueling innovations and driving technological breakthroughs in many areas. These range from biotechnology,[1,2] optics,[3] photonics,[4] electronics,[5] and energy,[6,7] to materials science.[8] Numerous synthesis routes of inorganic nanoparticles now exist in the literature and availability of small (<10 nm), fairly monodisperse and nonaggregated inorganic nanoparticle of various chemistries is no longer a constraint. The primary limitation of "solubility" or inorganic nanosol stability to perturbation from their "as synthesized" state during processing represents the critical challenge for any given application. The sols are extremely sensitive to changes in their physicochemical environment such as pH, ionic strength, temperature, and concentration often leading to aggregation. The need to offset the attractive *van der Waals* interaction that drives the aggregation of the particles is particularly significant for dense nanoscale inorganic particles with low interparticle minimum radial separations. This has been addressed through the adsorption of an organic layer (corona, shell, or adlayer) around the particle promoting an electrosteric or steric stabilization of the sol. This complexation is prevalent in organic solvents in the absence of charge. In addition to stabilization, the organic shell and/or the presence of some specific groups in the corona may also confer some functionality to the high surface area of the nanoparticles. Surface derivatization is crucial in biomedical applications like drug delivery, immunoassay, or cell imaging where the control of the interaction between the nanoparticles and biomacromolecules, cells, or living tissues drives toxicity.[1,9,10]

Metal-oxide nanocrystals such as cerium (CeO_2), iron (Fe_2O_3), zirconium (ZrO_2), and titanium (TiO_2) oxides represent a particularly important class of inorganic nanoparticles systems widely used in diverse technological areas. Despite this diversity in chemistry and application these particles share some common features. Their synthesis usually occurs in very acidic (or basic) environments by precipitation of metallic salts. The result is a stabilized sol at low pH (typically < pH 2) *via* electrostatic repulsion between particles. The main drawback is a very acute sensitivity to any variation of physicochemical conditions in the aqueous

*Address correspondence to jeanpaul.chapel@us.rhodia.com.

Received for review November 19, 2007 and accepted March 31, 2008.

Published online May 3, 2008.
10.1021/nn700374d CCC: $40.75

solution. To increase their stability range, low molecular weight molecules or ligands like citric acid[11] or poly(acrylic acid)[12] are generally used. The COOH groups of the ligands form complexes with the surface hydroxyl groups of the nanoparticles. At sufficiently high pH where the carboxylic groups are ionized (pH > 5), electrostatic stabilization of the sol occurs. The fundamental physical and chemical characteristics underlining the formation of the complexations are not straightforward since the complexations require some mechanical stress (shear, high energy ultrasounds)[13,14] to redisperse the sol or a two-step process (low pH aggregation−high pH redispersion[12]). The electrosteric repulsion conveyed *via* the ligands (*e.g.*, carboxylic groups) though less sensitive to perturbations of pH and/or ionic strength is still ionic. Compared to the bare sols it serves only to extend utility for application to a limited extent. The use of a head−tail architecture has been shown recently to be an efficient strategy for the dispersion of alumina nanoparticles[15] (polyethylene glycol or PEG tail and a gallol anchoring group) or the surface modification of yttrium oxide nanoparticles.[16] PEG oligomers can also be used as structure-directing agents to synthesize more complex structures.[17,18]

We report a facile complexation process giving rise to robust and versatile hybrid metal oxide nanoparticle sols with a well-anchored neutral corona for wide applicability. This process obviates the necessity for specialized processing steps as precipitation—redispersion. The choice of the complexing group(s), anchored on the particle surface, and the nature of the oligomeric tail, in the solvent, is of paramount importance. Among various anionic moieties it has been shown that phosphonic acid groups bind strongly to a variety of metal oxide surfaces at room temperature in aqueous solution.[16,19]

We also chose PEG groups that are widely used in biomedical applications to prevent nonspecific adsorption of proteins.[20] An end-grafted PEG layer may provide some biological stealth to the hybrid metal oxide particles.[21]

Along these lines, we highlight the potential and versatility of phosphonic-acid-terminated PEG oligomers to functionalize rare earth oxide nanoparticles. Cerium oxide is chosen to illustrate this approach because of its growing importance in science and technology ranging from material science (catalysis, polishing, optics, ...)[22−26] to biomedical[27−29] applications.

In the following section, we describe, characterize, and model the complexation process and the resulting nanostructure of the hybrid particles. We then underscore two key attributes of the tailored sol: (i) strong *UV absorption* capability after functionalization and (ii) ability to *redisperse* after freeze-drying as powder in *aqueous or organic solvents* in varying concentrations as singlet nanocolloids.

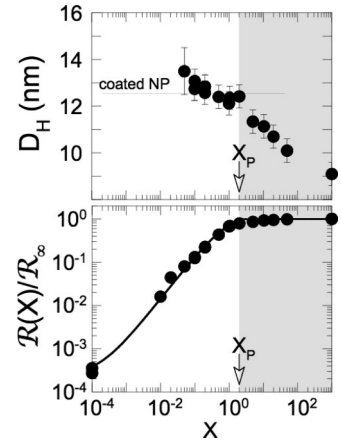

Figure 1. Rayleigh ratio and hydrodynamic radius D_H *vs* X at low pH (pH = 1.5). The continuous line is a fit to the data using a nonstoichiometric model for adsorption (see the analysis section). In the white region the fully covered particles coexist with free PPEG oligomers.

RESULTS AND DISCUSSION

Light Scattering. To understand and model the adsorption of the oligomers onto the nanoceria particles, hybrid solutions are prepared as a function of the volume ratio X defined in eq 7 with an overall concentration c kept constant. The Rayleigh ratios and hydrodynamic diameters are measured and plotted *versus* the mixing ratio X (Figure 1). $X = 10^{-4}$ corresponds to a solution containing phosphonated PEG oligomers (PPEG) only; $X = 1000$ corresponds to a solution containing bare nanoceria particles only. When X decreases from 1000 to 0.01, the size of the coated nanoceria increases gradually up to a critical value noted X_p where it then saturates around $D_H = 13$ nm. We interpret this result as the progressive coating of the particles by the oligomers until full coverage occurring at X_p. By further decreasing X, the number of fully covered particles decreases until their number is too low to be detected by dynamic light scattering (DLS) ($X \approx 0.01$). The normalized Rayleigh ratio (normalization by the Rayleigh ratio of the bare nanoceria R_{NP} ($X = \infty$)), as measured by static light scattering (SLS), is also monitored as a function of X. Here as well, one can clearly identify a critical ratio X equal to X_p where the Rayleigh ratio starts to decrease progressively with X. We interpret this result as the dilution of the fully covered particles by the free oligomers present in the bulk, in agreement with DLS results.

To confirm the existence of a critical volume ratio at X_p, below which particles are fully covered, the pH of the solutions is raised (it should be recalled that bare nanoceria solutions start to aggregate at pH = 3 and precipitate above pH = 5).[30] At pH = 9, a solution made at $X < X_p$ remains stable suggesting that the steric repulsion generated by the PEG layer is sufficient enough to prevent the destabilization of the sol. This result is confirmed by a Rayleigh ratio equal to the value found at pH = 1.5. Above X_p, as expected, the solution begins

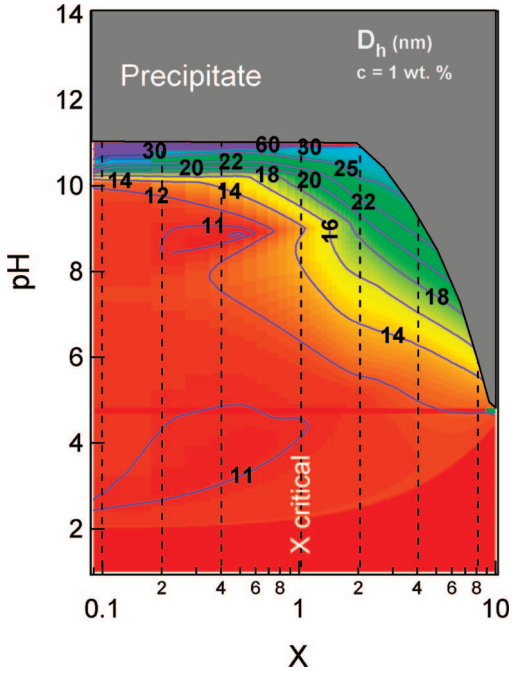

Figure 2. Stability phase diagram of the PPEG-CeO_2 nanoparticles: hydrodynamic radius D_H *vs* X and pH. The grey region represents visible phase separation. Contours and colors (red to blue) indicate D_H variation from 10 to 40 nm.

to aggregate owing to the lack of oligomers on the particles resulting in a very low steric hindrance.

Furthermore, a comprehensive description of the behavior of the coated particles as a function of *pH* and *mixing ratio X* is undertaken. A large number of different experimental conditions are gathered in Figure 2 representing the whole stability phase diagram of the CeO_2−PPEG hybrid nanoparticles. As the pH is progressively increased, the solutions become destabilized at pH > 10.5. This critical upper stability limit is identical to the pK_a of the (110) and the (111) facet of the ceria nanocrystal unit cell when the charge changes from zwitterionic to negative.[30] We postulate desorption of the phosphonated-PEG at this pH due to the coincidence of the transition to the aggregated state. Another feature of this phase diagram is the existence of a general critical $X = X_p$. For all values of $X > X_p$, the particle size increases progressively at a lower pH leading to early phase separation.

To obtain more quantitative results on this system, the Rayleigh ratios were measured at pH = 1.5 for both CeO_2 and CeO_2−PPEG dispersions as a function of the CeO_2 weight fraction (Figure 3).

The two slopes are different because the Rayleigh ratio is proportional to K and M_W, as shown in eq 10. The slopes of the linear regressions for the CeO_2−PPEG and CeO_2 Rayleigh ratios *versus* the CeO_2 weight fraction are 0.1284 and 0.0743, respectively. The clear difference in the two slopes gives us the possibility to precisely compute the number of adsorbed PPEG chains per nanoceria. Using expression (1) described in a former

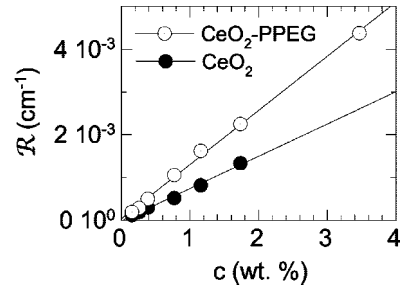

Figure 3. Rayleigh ratios of CeO_2 and CeO_2−PPEG solutions *versus* the CeO_2 weight fraction.

publication[12] and values from Table 1 one finds 270 ± 30 phosphonated-PEG per CeO_2 particle.

$$\frac{R^{CeO_2-PPEG}}{R^{CeO_2}} = \frac{K^{CeO_2-PPEG}}{K^{CeO_2}}\left(1 + n_{ads}\frac{M_W^{PPEG}}{M_W^{CeO_2}}\right)^2 \qquad (1)$$

The molecular weight of a hybrid nanoparticle is hence M_w = 440 ± 30 Kg/mol. The organic layer represents 38% of the total weight.

The determination of the mutual diffusion coefficients for both dispersions at different weight fractions allows for the calculation of D_0, the self-diffusion coefficient (see Materials and Methods) of the bare and coated nanoparticles (Figure 4). Careful DLS measurements are able to distinguish a different behavior for coated and noncoated particles. Using the Stokes−Einstein relation, the hydrodynamic diameters D_H of bare and PPEG-coated nanoparticles were found to be D_H = 9.2 nm and D_H = 12.3 nm, respectively. One can estimate a thickness of 1.6 nm for the PPEG corona. The theoretical fully extended contour length of the PPEG molecules is about 4.5 nm. The difference expresses the grafting density of the PPEG onto the particle (270 chains per particles or 1 chain/nm^2) typical for oligomers adsorbing onto nanoparticles[15] (the nonspherical shape of the particle might also play a role). A monolayer of PPEG densely grafted (and fully stretched) would give a grafting density of 3.5 chains/nm^2 PPEG. The nonfully stretched configuration of the PPEG is however sufficient to provide a very good steric stabilization.

Nonstoichiometric Model. Two mechanisms that describe how polymers coat nanoparticles have been con-

TABLE 1. Molecular Weight (M_w), Refractive Index Increment (dn/dc), Hydrodynamic Diameter (D_H), Light Scattering Coupling Constant K (at 632.8 nm), Characterizing PPEG Oligomer, the Nanoceria, and the PPEG-Coated Nanoceria Investigated in the Present Work[a]

specimen	dn/dc (cm^3 · g^{-1})	K (632.8 nm) (cm^2 · g^{-2})	M_w (g · mol^{-1})	D_H (nm)	R_g (nm)
PPEG	0.102	7.58 10^{-8}	624	—	—
CeO_2	0.192	2.69 10^{-7}	269000	9.2	3.2 ± 0.1[a]
CeO_2−PPEG	0.154	1.72 10^{-7}	439000	12.3	4.4 ± 0.1[a]

[a]The gyration radii (R_g) were measured by SANS.

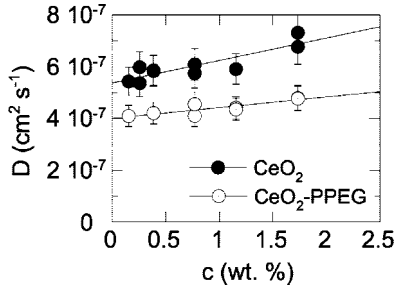

Figure 4. Mutual diffusion coefficient *versus* CeO_2 weight fraction in CeO_2 and CeO_2−PPEG dispersions. The extrapolation of the straight lines at $C = 0$ gives D_0.

sidered to model the adsorption of the PPEG oligomers onto the particles. The mechanisms named stoichiometric (ST)[31] and nonstoichiometric (NST) models[32] (Figure 5) are described in the literature. The main difference between them only appears above X_p ($X > X_p$) where the particles are no longer fully covered (shortage of oligomers). Two distinct mechanisms are likely. In the first, the coated nanoparticles coexist with noncoated ones giving a number of oligomers/particle n_{ads} constant throughout the X range (ST model). In the second, all nanoparticles are equally covered (NST model) and n_{ads} is hence a function of X. Below X_p ($X < X_p$) where the two models merge, the coated nanoparticles coexist with free oligomers present in the bulk solution.

From a closer look to the data of Figure 1, and within the experimental error of the light scattering technique, D_H appears quite constant (around 13 nm) up to a value of X close to X_p when it starts to drop smoothly until it reaches the value of the bare nanoceria particle (9.2 nm) at $X = \infty$ (extreme point on the right). This behavior suggests a NST model for the adsorption. In addition, no precipitation above X_p is seen in the phase diagram (Figure 2) for pH < 5. This result is in contradiction with a ST model that would predict the coexistence between bare and coated particles leading to the aggregation of a portion of the sol. Therefore, a nonstoichiometric adsorption mechanism is selected to model the oligomer adsorption onto the nanoparticles. In what follows, the X-dependence of the scattered intensity will be modeled accordingly.

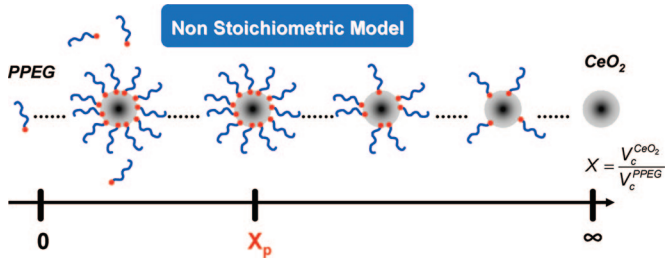

Figure 5. Schematic representation for the nonstoichiometric adsorption mechanism of phosphonated-PEG onto nanoceria particles. Below the critical volume ratio X_p, the particles are fully covered and in equilibrium with a decreasing number of nonadsorbed oligomers. Above X_p, the number of grafted oligomers progressively decreases toward bare particles ($X = \infty$). At X_p, all the oligomers present in the initial solution are adsorbed onto the particle.

In the experiments described previously, the total concentration c of active matter (CeO_2 + PPEG) is kept constant. The respective nanoparticles and oligomers concentrations are given by eq 7 regardless of any interaction between them. One can define the nominal number of oligomers/particle as $n_{ads}(X) = M_w^{CeO_2}/(XM_w^{PPEG})$. Below X_p, n_{ads} is equal to $n_{ads}(X_p)$, and the solution contains fully coated nanoparticles (CeO_2) and free oligomers (PPEG). Above X_p, n_{ads} is a function of X and the solution contains only partially covered particles. The total scattering intensity expresses hence as the sum of different contributions. As a result, the Rayleigh ratio normalized to its value at $X = \infty$ ($R = K^{CeO_2}M_w^{CeO_2}c$) reads as

$$\tilde{R}(X<X_p) = \tilde{K}M\left(\frac{X_p - X}{X_p(1+X)}\right) + \left(\frac{\sqrt{\tilde{K}}+X_p}{X_p}\right)^2\left(\frac{x}{1+x}\right) \quad (2)$$

The first term arises from the free oligomers present in the bulk, and the second term arises from the fully covered particles. Similarly, at high X the contribution arises solely from the partially covered particles and the intensity goes as

$$\tilde{R}(X>X_p) = \left(\frac{1+X}{X}\right)\left(\frac{\sqrt{\tilde{K}}+X}{1+X}\right)^2 \quad (3)$$

where $\tilde{K} = K^{PPEG}/K^{CeO_2}$ and $M = M_w^{PPEG}/M_w^{CeO_2}$.

When X goes either to zero (only oligomers in the solution) or to infinity (only nanoparticles), the ratio tends, as expected, to $\tilde{K}M$ or 1, respectively. The normalized Rayleigh ratios do not depend on the total concentration c; therefore the expression should be valid at all concentration in the dilute regime. Equations 2 and 3 are used to fit the scattering data of Figure 1 with X_p as the sole adjustable parameter. All other quantities such as the coupling constant $\tilde{K}$, and the molecular weights of both oligomers and nanoparticles are known. The result of the fitting is shown in Figure 1 as a solid curve. The agreement between the model and the data is excellent. X_p is found to be 1.65 leading to a number of oligomers/particle $n_{ads}(X_p) = 260 \pm 30$ in close agreement with the results found through the data of Figure 3.

SANS Scattering. To complement light scatterings data, SANS is performed on both bare and PPEG-coated nanoparticles to investigate the nanostructure of the core−shell hybrid system (Figure 6). The scattered intensity $I(q)$ of spherical objects can be decomposed into a structure factor $S(q)$ and form factor $P(q)$. At sufficiently low concentration (<1 wt %), the structure factor is equal to 1 (no interparticle interaction), the scattered intensity is proportional to the concentration and the q-dependence of the intensity reflects the form fac-

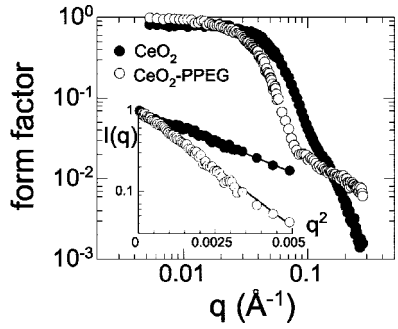

Figure 6. SANS form factor $P(q)$ for bare and coated nanoparticles in double logarithmic scale. The inset shows the Guinier representation of the intensity for the same samples ($I(q)$ *versus* q^2). From the straight lines, the gyration radii for bare and coated nanoceria were calculated, R_g = 3.2 and 4.4 nm, respectively.

tor $P(q)$ of the aggregates. Figure 6 shows the form factor of both bare and modified particles. Because the measurements of the scattered intensity are performed in H_2O and D_2O for the CeO_2 and PPEG-CeO_2 system, respectively, the curves at high q cannot be superimposed. The extra contribution to the scattered intensity due to the presence of the organic layer is, however, clearly seen at low q in the Guinier representation where $R_g q < 1$ (inset Figure 6). Here, the logarithm of the intensity decreases linearly with q^2 and from the straight lines, we deduce a radius of gyration $R_g = 3.2 \pm 0.1$ nm for the bare nanoparticles and $R_g = 4.4 \pm 0.1$ nm for the PPEG-coated ones. For homogeneous and monodisperse spheres of radius R, $R = R_H = 1.29\ R_g$. In the present case, for the bare particles, we find $R_H/R_g \approx 1.44$. The discrepancy likely reflects the polydispersity in size of the cerium oxide particles. In the Porod representation ($I(q) * q^4$, not shown here), the first oscillation of the form factor shifts toward lower q after the coating (from 0.11 to 0.07 $Å^{-1}$) supporting the presence of the organic layer. However, because of polydispersity it is difficult to extract the radius R of the particles ($q^{\text{first minimum}} R = 4.57$). In addition, from experiments performed with solutions having different H_2O/D_2O volume ratios it is possible to measure the average scattering length density ($\tilde{\rho}$) of the bare and coated particles. The plot of $(I(q\to0)/c)^{1/2}$ as a function of the proportion

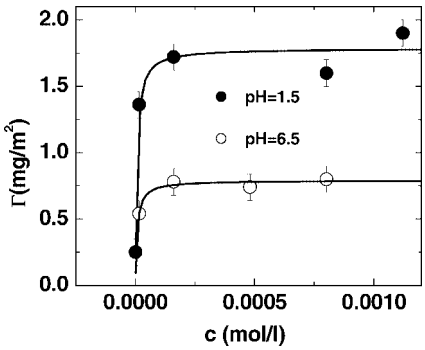

Figure 7. Adsorption isotherms $\Gamma(c)$ of PPEG oligomers onto model CeO_2-coated substrates at low (1.5) and neutral pH (6). The solid curve is the Langmuir fit to the data.

of H_2O in the ($H_2O + D_2O$) mixed solution gives a straight line (not shown here). The ratios that cancel out the intensity correspond to $\tilde{\rho}$. We find $\tilde{\rho}_{CeO_2} = 4.99 \times 10^{10}$ cm^{-2} for the bare particles. In the case of coated ones the ratio gets rather through a minimum (because it is not possible to match jointly the particle and the organic shell) giving $\tilde{\rho}_{CeO_2\text{-PPEG}} = 1.93 \times 10^{10}$ cm^{-2}.

From the results gathered so far, the coated nanoparticles seem to have a hybrid core−shell structure. In that case, the intensity excess as $q \to 0$ due to the PPEG shell can be approximated by[12]

$$\left(\frac{I^{CeO_2-PPEG}}{I^{CeO_2}}\right)_{q\to0} = \left(1 + n_{ads}\frac{\tilde{\rho}^{PPEG} - \tilde{\rho}^{D_2O}}{\tilde{\rho}^{CeO_2} - \tilde{\rho}^{D_2O}}\frac{v_M^{PPEG}}{v_M^{CeO_2}}\right)^2 \quad (4)$$

The ratio on the left side of eq 4 was found experimentally. The intensity scattered by the coated ceria was 38 times that of bare particles in D_2O. Knowing $\tilde{\rho}_{CeO_2}$, the molar volume of bare ceria $v_M^{CeO_2}$ can also be calculated from the intensity scattered as $q \to 0$ of a diluted ceria solution. The molar volume of a PPEG oligomer is estimated *via* its M_w and a bulk density of 1.13 ($v_M^{PEG} \approx 910$ $Å^3$). The values of ρ^{D_2O} ($= 6.33 \times 10^{10}$ cm^{-2}) and ρ^{PEG} ($= 0.84 \times 10^{10}$ cm^{-2}) are classically computed according to their composition and density. Finally, one ends up with a number of adsorbed PPEG oligomers/particle $n_{ads} = 230 \pm 30$.

Both light and neutron scattering data are in very good agreement, confirming the consistency of our approach and the accuracy of the results. From quantitative scattering data we are able to deduce the main features of the core−shell nanostructure of the hybrid particles. The integrity and efficiency of the coating process is also highlighted. The PPEG functionalization does not alter the main specificities of the original sol, for example, singlet nanometer-sized cerium oxide particles, and greatly expands its stability range up to pH = 9.

Adsorption Isotherms. To evaluate the affinity of the phosphonated-PEG oligomers with the surface of cerium oxide nanoparticles, adsorption isotherms are measured on macroscopically flat CeO_2 model surfaces with the help of optical reflectometry. As seen in Figure 7, in both values of pH investigated, the curves present a rather sharp increase of the adsorbed amount at very low concentration. This rapid flattening out of the adsorbed amount suggests a rather high affinity of the oligomers toward cerium oxide surface. The data of Figure 7 can be fitted using a Langmuir[15] model where the oligomers adsorbed amount $\Gamma(c)$ reads

$$\Gamma(c) = \frac{k\Gamma_{sat}c}{1 + kc} \quad (5)$$

where Γ_{sat} is the maximum adsorbed amount, c is the (equilibrium) concentration of oligomers in the aque-

ous solution, and k is the adsorption constant ($= k_{adsorption}/k_{desorption}$). The fit gives values of $\Gamma_{sat} = 1.8$ mg/m^2, $k = 1.6 \times 10^5$ L/mol and $\Gamma_{sat} = 0.8$ mg/m^2, $k = 1.4 \times 10^5$ L/mol for pH = 1.5 and pH = 6.5, respectively. In both cases k is quite large leading to small values for $k_{desorption}$, consistent with a high affinity type of isotherm. The magnitudes of the adsorbed amounts are typical for organic matter adsorbing onto inorganic surfaces. The adsorbed amount (at pH = 1.5) computed from light scattering results ($D_H = 9.2$ nm, 270 oligomers/NP) is equal to 1.1 mg/m^2 (assuming a spherical shape for the NP). Hence, both approaches agree reasonably well. In addition, due to a size comparable to a nanoparticle, an oligomer adsorbing on top of the ceria model surface does not see a homogeneous layer, but rather a compact set of nanoceria spheres with at most a 90% coverage (in the case of an hexagonal close-packing). This layer develops a surface area of $2\pi R^2 \times$ number of particles (the surface area of hemispheres of radius R). The renormalized adsorbed amount is $\Gamma^*1.1/2 \approx 1$ mg/m^2 in very good agreement with the value found through light scattering experiments.

The free energy of adsorption ΔG^{ads} of the PPEG oligomers on the ceria surface is estimated from the following expression:

$$\Delta G^{ads} = -k_B T \ln\left(\frac{k}{V^m_{water}}\right) \quad (6)$$

where k_B is the Boltzmann constant, T is the temperature, and V^m_{water} is the molar volume of water (0.018 L/mol).[33,34] The adsorption free energies are found to be $-16\, k_B T$ and $-15.8 k_B T$ for pH = 1.5 and pH = 6.5, respectively. Though the exact nature of the bond between PPEG and ceria is not known at this stage, the measured free energies might indicate an adsorption mechanism controlled by electrostatic interaction.[15] At pH = 1.5 the ceria nanoparticles are cationically charged (Ce-OH$_2^+$) and the PPEG are only slightly anionic (3%, p$K_1 \approx 2.7$). However, it has been reported[35,36] in the literature that the presence of oppositely charged nanoparticles can affect considerably the acid-basic properties of weak poly acid by making group or chain ionization easier. Although we do not know at this stage how to quantify such mechanism, it can possibly apply in our system and explain the presence of a larger charge on the weak phosphonic acid at low pH leading to the strong adsorption measured.

At pH = 6.5, close to its isoelectric point (IEP), ceria nanoparticles are less cationic and PPEG oligomers are 50% anionically charged (p$K_2 \approx 7.8$). The lower amount measured at higher pH may be due to electrostatic repulsion between the charged oligomers while adsorbing onto the surface. At this pH, the presence of more than one charged group in the phosphonated head could possibly force the oligomers into a flatter configuration leading to a lower adsorbed amount as well. The acid-basic interaction between the hydroxyl groups (Ce-OH) of the ceria and the remaining phosphonic acid groups (O═P−(OH)) of the PPEG might also favor adsorption leading possibly to a Ce−O−P═O bond with the release of a H_2O molecule. The reactivity of phosphonic acid groups toward metal oxide surfaces is known to correlate with its basicity.[37] In the case of yttrium oxide (Y_2O_3) nanoparticles (yttrium and cerium are rare earth elements with similar electronegativity and ionic radii)[38] the "condensation" takes place at room temperature.[16] Furthermore, the modified CeO_2 sol was able to withstand a week-long dialysis against pure water without aggregating, highlighting the robustness of the organic coating. It should be noted finally that at very high pH (>11), the sol precipitates as can be seen in the phase diagram of Figure 2. This observation indicates a possible hydrolysis of Ce−O−P bonds in the aggressive alkaline environment as the ceria surface changes from zwitterionic to anionic.[30] The adsorption results give evidence of the specificity of a phosphonated oligomer to create a robust metal oxide hybrid sol.

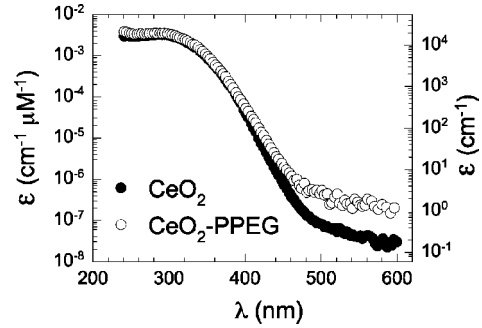

Figure 8. UV−visible spectra of bare and coated nanoceria.

Benefits: UV Absorption and Redispersible Nanopowders. The data and models offer a clear insight into the formulation process and the nanostructure of the modified hybrid nanoparticles and translate into two valuable bulk properties of the new sol: UV absorption and the creation of redispersible nanopowders by freeze-drying the nanosol.

One of the well-known characteristic properties of cerium oxide particles is strong UV absorbance with minimal absorbance in the visible regime. However, given the large surface area once covered with an organic layer and the possibility to form metal−ligand charge transfer complexes this unique property may be adversely affected. We undertook UV−visible measurements to rule out this hypothesis. As seen in Figure 8, both bare and coated nanoceria have the same absorbance variation through the entire UV−visible region. This result is valuable because the robustness of the PPEG-ceria nanoparticle sol that has been investigated in this work has direct impact for applications where anti-UV protection is needed.

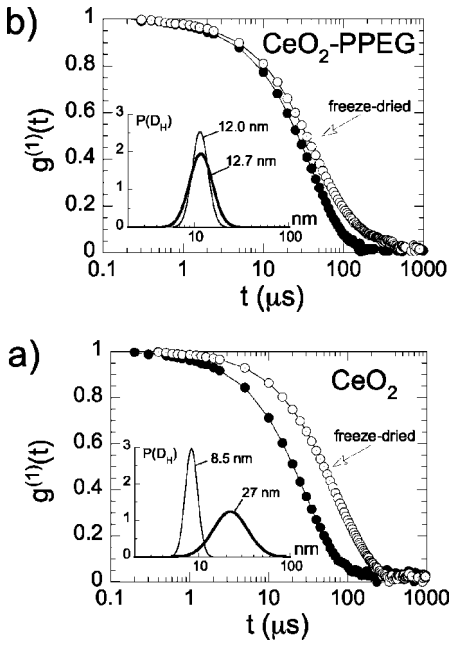

Figure 9. Redispersion in aqueous solutions of CeO_2 and PPEG-CeO_2 powders obtained by freeze-drying both stock solutions. (a) Correlation functions of the original sol before and after freeze-drying and redispersion. The inset shows the derived hydrodynamic radii D_H distribution. (b) *id.* hybrid sol. For sake of comparison, the diffusion coefficients have been measured at a concentration of 0.1%. They have not been extrapolated to zero concentration leading to slightly smaller D_H values than in Table 1.

Another test for the robustness of the surface modification and the ability to prepare stable concentrated solutions was evaluated by drying the hybrid nanosol. A second important matter is the possibility to handle powders rather than solutions to improve the shelf life expectancy or simply to prepare solutions in a different solvent.

To further investigate this idea, we freeze-dried (Freezone model, Labconco, Kansas City, MO) bare and hybrid nanoceria solutions for 48 h to remove any trace of the water. The phosphonated-PEG ceria solution was dialyzed (5K membrane) against DI water prior to freeze-drying, to remove any free PPEG oligomers present in the bulk.

Aliquots of the freeze-dried powders so prepared when added to water showed a remarkable result that the hybrid nanosols appeared to readily redisperse to give clear solutions when compared to bare nanoparticles which evidenced a slightly milky appearance. Both powders were redispersed in aqueous solutions at pH = 1.5 for bare particles and DI water for stabilized particles and stirred overnight. Figure 9 shows the correlation functions measured with dynamic light scattering (at 90°) of the original and modified sol before and after redispersion. The distributions $P(D)$ of the hydration diameters D_H are also shown (inset Figure 9). After redispersion, the correlation function of the bare CeO_2 solution is clearly shifted toward longer times. As a result, the mean D_H is shifted toward larger values together with a clear broadening of the distribution ($D_H = 26.8 \pm 11.4$ nm) compared to the small and slightly polydisperse particles in the original solution ($D_H = 8.5 \pm 0.8$ nm). Freeze-drying the *reactive* bare CeO_2 particles would likely have led to some condensation among the Ce-OH groups present on their surfaces giving rise to larger aggregates. In the case of *passivated* PPEG-CeO_2 particles, the freeze-drying process did not significantly change the original distribution indicating no change in the surface complexation of PPEG during the drying process. Both correlation functions are almost superimposed giving a very similar distribution of D_H ($D_H = 12 \pm 0.1.4$ and $D_H = 12.7 \pm 1.5$). This redispersibility is only possible for compositions where $X < X_p$. This hybrid metal oxide nanopowder has ability to overcome strong van der Waals attractions by hydration/solvation of the PPEG corona yielding singlet nanocolloids while the formation of the barrier coating at the particle interface protects against interparticle chemical condensation. This has clear implications for the utility of nanoceria providing clear cost and processing advantages in allowing shipping of nanopowders rather than dilute solutions and in the preparation of stable concentrated solutions for bulk applications.

The sol stability and redispersability were further extended through the choice of the complexing oligomer backbone. The hybrid metal oxide powder is *also redispersible in certain organic solvents* like ethanol, acetone, or chloroform (not shown here) which is not the case for bare particles. These results may easily be extended to other nanoparticle systems. The complexation of nanoceria with end-functional PPEG to create true redispersible nanopowders in aqueous or certain organic solvents provides the framework for designing a truly versatile hybrid metal oxide sol with clear utility in a range of applications.

CONCLUSION

The generation of robust and versatile phosphonated-PEG cerium oxide nanoparticles is highlighted through a detailed series of complementary experiments. From quantitative light and neutron scattering data we are able to obtain the main features of the CeO_2−PPEG hybrid core−shell nanostructure and to model the adsorption mechanism (NST model). The microstructure is described in terms of molecular weight M_w, hydrodynamic diameter D_H, and number of adsorbed oligomers per particle N_{ads}. The characteristic evolution of the Rayleigh ratio as a function of the mixing ratio is successfully described in term of nonspecific adsorption of oligomers onto nanoparticles. The NST model evidenced the presence of a critical ratio X_p at which the particles are fully covered with an average number of chains $N_{ads} = 270$. Beyond that threshold, the organic coating progressively diminishes, increasing the sensitiveness of the sol toward destabilization.

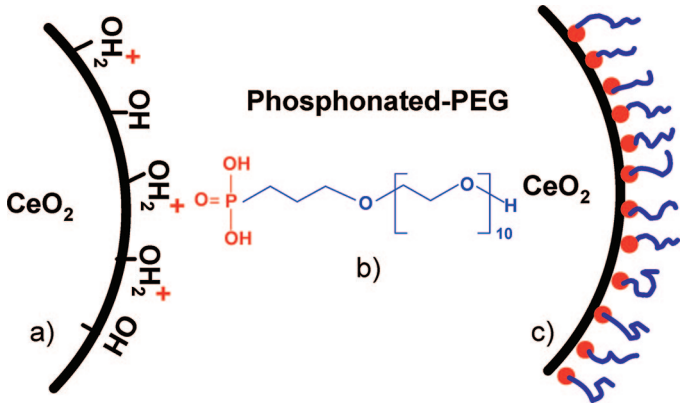

Figure 10. (a) Simplified sketch of the surface chemistry of cerium oxide nanoparticles: cationic protonated hydroxyl groups *versus* neutral hydroxyl groups. (b) Tailored phosphonated-PPEG chemical architecture for the adsorption onto nanoparticles: reactive phosphonate head + neutral PEG tail. (c) Phosphonated-PEG corona around the particle: steric stabilization + PEG functionality.

In addition, the measurement of the free energy of adsorption ΔG^{ads} (*ca.* $-16kT$) has shown that electrostatic interaction is likely the main driving force the complexation which eventually increased the affinity of the phosphonate anchoring groups toward the CeO_2 surface.

The main specificities of the original sol are not altered during the functionalization phase leading to nanometer-sized cerium oxide particles covered with a well-anchored layer of PEG chains. This solvating brush-like layer is sufficient to solubilize the particles and greatly expands the stability range of the original sol up to pH = 9. These results highlight the specificity of the terminus phosphonate group to create a robust metal oxide hybrid sol. Furthermore, tailoring the oligomer architecture with both a noninteracting PEG tail and a monofunctional phosphonate head prevented colloidal bridging emphasizing the advantage of the current functionalization route over other ones using multisticker binding. Some direct benefits of such hybrid sols are finally put forward. After functionalization, they maintain a strong UV absorption capability, a very valuable characteristic for applications where anti-UV protection is needed. Moreover, after freeze-drying the hybrid particle solution, the powder was able to *redisperse* in different solvents without losing any of its features conferring a great versatility and ease of use of the CeO_2−PPEG nanoparticles in dry or wet conditions. Beside their bulk properties described in this paper, the hybrid nanoparticles present some very interesting interfacial properties that will be discussed in a forthcoming publication.

MATERIALS AND METHODS

Oligomers and Nanoparticles. The phosphonated poly(oxyalkene) investigated in this work is a proprietary oligomer (poly(oxy-1,2,ethanediyl)-α-(3-phosphonopropyl) omega hydroxyl or 3-phosphonopropyl alcohol ethoxylate-10 EO), produced by Rhodia Inc. and named hereafter phosphonated-PEG or PPEG (Figure 10). Titration curves with NaOH (1 M) show the presence of two distinct p*K*a values for this weak diacid at $pK_{a1} = 2.7$ and $pK_{a2} = 7.8$.

The inorganic mineral oxide nanoparticle system investigated is a dispersion of cerium oxide nanocrystals, or nanoceria sol at pH 1.5. The synthetic procedure involves thermohydrolysis of an acidic solution of cerium-IV nitrate salt ($Ce^{4+}(NO_3^-)_4$) at high temperature (70 °C), that results in the homogeneous precipitation of a cerium oxide nanoparticle pulp ($CeO_2(HNO_3)_{0.5}(H_2O)_4$).[39] The size of the particles was controlled by the addition of hydroxide ions during the thermohydrolysis. High resolution transmission electron microscopy has shown that the nanoceria (bulk mass density $\rho = 7.1$ g cm^{-3}) consists of isotropic agglomerates of 2−5 crystallites with a typical size of 2 nm and faceted morphologies. Wide-angle X-ray scattering has confirmed the crystalline fluorite structure of the nanocrystallites (see Supporting Information).[40] Image analysis performed on cryo-TEM images of single nanoparticles have shown a polydispersity index $s = 0.15 \pm 0.03$ for the particles (s is defined as the ratio between the standard deviation and the average diameter).[41]

As synthesized, the cerium oxide nanosols are stabilized by a combination of long-range electrostatic forces and short-range hydration interactions (including strongly bound or condensed nitrate ions). At such pH, the ionic strength arises from the residual nitrate counterions present in the solution and acidic protons. This ionic strength around 0.045 M gives a Debye screening length $K_D^{-1} \approx 1.5$ nm. An increase of the pH *or* ionic strength (>0.45 M) results in a reversible aggregation of the particles and destabilization of the sols leading eventually to a macroscopic phase separation. Though the change in pH apparently reduces the effective surface charge of the particles, it also reduces the range of the electrostatic repulsion. For this system, the destabilization of the sols occurs well below the point of zero charge of the ceria particles, pzc = 7.9.[30] The bare nanoceria particles have a zeta potential $\zeta = +30$ mV and an estimated structural charge of $Q_{CeO_2} = +300$ e. The charges are compensated by nitrate anions in the Stern and diffuse layers surrounding each particle.

Hybrid Nanoparticles Formulation. The pH of the PPEG solution is adjusted with reagent-grade nitric acid (HNO_3). Mixed solutions of nanoparticles (CeO_2) and phosphonate-PEG (PPEG) are prepared by simple mixing of dilute solutions prepared at the same concentration c ($c = 0.1-1$ wt %) and same pH. This ensures that no aggregation of nanoparticules occurs owing to pH or salinity gap. At pH = 1.4, 2.5 wt % of the phosphonate groups are ionized. The relative amount of each component is monitored by the volume ratio X, yielding for the final concentrations

$$c_{CeO_2} = \frac{cX}{1+X}, \quad c_{PPEG} = \frac{c}{1+X} \tag{7}$$

Ammonium hydroxide (NH_4OH) is used to adjust the pH of CeO_2−PPEG dispersions in the range of 1.5−10.

Static and Dynamic Light Scattering. Static and dynamic light scattering (SLS) measurements are performed on a BI-9000AT Brookhaven spectrometer (incident wavelength 488 nm) and on a Zetasizer Nano ZS from Malvern. Rayleigh ratios R and hydrodynamic diameters are measured as a function of the concentration c. R is obtained from the scattered intensity $I(c)$:

$$R(q,c) = R_{std}\frac{I(c) - I_S}{I_{TOL}}\left(\frac{n}{n_{TOL}}\right)^2 \tag{8}$$

where R_{std} and n_{Tol} are the standard Rayleigh ratio and refractive index of toluene; I_S and I_{Tol} are the intensities measured for the solvent and for the toluene in the same scattering configuration. Light scattering is used to determine the apparent molecular weight $M_{W,app}$ (the gyration radius R_g was determined by

neutron scattering) of colloids investigated here. In the regime of weak colloidal interactions, the Rayleigh ratio $R(c)$ is found to follow concentration dependence:

$$\frac{Kc}{R(q,c)} = \frac{1}{M_{w,app}}\left(1 + \frac{q^2R_g^2}{3}\right) + 2A_2c \quad (9)$$

where $K = 4\pi^2n^2 (dn/dc)^2/N_A\lambda^4$ is the scattering contrast coefficient (N_A is the Avogadro number) and A_2 is the second virial coefficient. The refractive index increments dn/dc of the different solutions are measured using a Bellingham & Stanley model RFM840 refractive index detector in the range $c = 10^{-3}$ to 1 wt %. The values of the refractive index increments and K coefficients for the oligomers and nanoparticles solutions are shown in Table 1. For the oligomers and the nanoparticles in the dilute concentration range ($c < 1$ wt %), $qR_g \ll 1$, eq 9 reduces to

$$R(c) = KM_{w,app}c \quad (10)$$

This expression emphasizes the fact that for small sizes ($< \lambda/20$), the Rayleigh ratio does not depend on the wave-vector in the window 6×10^{-4} to 4×10^{-3} Å^{-1}, characteristic for light scattering.

To accurately determine the size of the colloidal species, dynamic light scattering (DLS) was performed with concentrations ranging from $c = 0.01$ to 1 wt %. In this range, the diffusion coefficient varies according to $D(c) = D_0(1 + D_2c)$, where D_0 is the self-diffusion coefficient and D_2 is a virial coefficient of the series expansion. The sign of the virial coefficient, the type of interactions between the aggregates, either repulsive or attractive can be deduced. Here D_2 is positive ($+10^{-7}$ cm$^2 \cdot$ s^{-2}), indicating a repulsive interparticle interaction. From the value of $D(c)$ extrapolated at $c = 0$ (noted D_0), the hydrodynamic radius of the colloids is calculated according to the Stokes−Einstein relation, $D_H = k_BT/3\pi\eta_SD_0$, where k_B is the Boltzmann constant, T is the temperature ($T = 298$ K), and η_S ($\eta_S = 0.89 \times 10^{-3}$ Pa $\cdot$ s) is the solvent viscosity. The autocorrelation functions of the scattered light are interpreted using both the method of cumulants and the CONTIN fitting procedure provided by the instrument software.

UV−visible Absorption Spectrometry. A UV−visible spectrometer (SmartSpecPlus from BioRad) is used to measure the absorbance of bare and coated nanoceria dispersion in water. The absorbance is related to the nanoparticle concentration by the Beer−Lambert expression:

$$\text{Abs} = \varepsilon\,\ell\,c_{NP} = -\log T \quad (11)$$

where ℓ (=1 cm), is the optical length of the cell, c_{NP} is the nanoparticle concentration, ε is the molar absorption coefficient (cm$^{-1} \cdot \mu$M^{-1}), and T is the transmission. In the following, the nanoparticle concentration will be expressed in wt % or in μM of cerium oxide.

Optical Reflectometry. The adsorption isotherms $\Gamma(c)$ of PPEG oligomers onto a cerium oxide model surface is monitored using optical reflectometry.[42,43] Fixed angle reflectometry measures the reflectance at the Brewster angle on the flat substrate. A linearly polarized light beam is reflected by the surface and subsequently split into a parallel and a perpendicular component using a polarizing beam splitter. As material adsorbed at the substrate−solution interface, the intensity ratio S between the parallel and perpendicular components of the reflected light is varied. The change in S is related to the adsorbed amount through

$$\Gamma(t) = \frac{1}{A_s}\frac{S(t) - S_0}{S_0} \quad (12)$$

where S_0 is the signal from the bare surface prior to adsorption. $\Gamma(c)$ is constructed by taking the plateau value $\Gamma_{Plateau}$ of a given $\Gamma(t)$ curve at different concentrations c ($c = 0.001-0.1$ wt %). A complete description of the stagnation point adsorption reflectometry device can be found in several references.[43–48]

CeO$_2$ Model Surfaces. A thin layer of polystyrene of ~100 nm is deposited on top of an HMDS (hexamethyldisilizane) functionalized silicon wafer by spin-coating a toluene solution (25 g/L) at 5000 rpm.[49] The surface is then dipped in a nanoceria solution (0.1 wt %) containing 0.1 M $NaNO_3$ overnight. This results in the formation of a well-packed nanoceria monolayer on top of the PS surface as seen by AFM imaging (not shown here). Bare particle adsorption on plastic surfaces will be described in a forthcoming publication. It should be noted that the receding water contact angle θ_r on such a model nanoceria surface was below 15° in contrast with a $\theta_r = 85°$ for the original PS surface.

Small-Angle Neutron Scattering. Small-angle neutron scattering (SANS) spectra are measured on a PAXY spectrometer (Laboratoire Leon Brillouin-LLB, Saclay, France). Two configurations are used ($D = 1.35$ and 6.70 m, both at $\lambda = 6$ Å), covering a q-range from 5×10^{-3} to 0.2 Å^{-1}. Exposure times of 2 and 1 h for the small and large angle configuration, respectively, are necessary to obtain good statistics. Raw data are radially averaged. Standard corrections for sample volume, neutron beam transmission, empty cell signal subtraction, and detector efficiency have been applied to get the scattered intensities in absolute scale using standard LLB software.

Supporting Information Available: WAXS and HR-TEM data for bare CeO_2 particles. This material is available free of charge *via* the Internet at http://pubs.acs.org.

REFERENCES AND NOTES

1. Rabin, O.; Perez, J. M.; Grimm, J.; Wojtkiewicz, G.; Weissleder, R. An X-Ray Computed Tomography Imaging Agent Based on Long-Circulating Bismuth Sulphide Nanoparticles. *Nat. Mater.* **2006**, *5*, 118–122.
2. Huang, X. L.; Bronstein, L. M.; Retrum, J.; Dufort, C.; Tsvetkova, I.; Aniagyei, S.; Stein, B.; Stucky, G.; Mckenna, B.; et al. *Nano Lett.* **2007**, *7*, 2407–2416.
3. Konstantatos, G. E. A. Ultrasensitive Solution-Cast Quantum Dot Photodetectors. *Nature* **2006**, *442*, 180.
4. Zheludev, N. I. Single Nanoparticle as Photonic Switch and Optical Memory Element. *J. Optic. Pure Appl. Optic.* **2006**, *8*, S1−S8.
5. Boettcher, S. W.; Strandwitz, N. C.; Schierhorn, M.; Lock, N.; Lonergan, M. C.; Stucky, G. D. Tunable Electronic Interfaces between Bulk Semiconductors and Ligand-Stabilized Nanoparticle Assemblies. *Nat. Mater.* **2007**, *6*, 592–596.
6. Gur, I.; Fromer, N. A.; Geier, M. L.; Alivisatos, A. P. Air-Stable All-Inorganic Nanocrystal Solar Cells Processed from Solution. *Science* **2005**, *310*, 462–465.
7. Wang, P. E. A. A Stable Quasi-Solid-State Dye-Sensitized Solar Cell with an Amphiphilic Ruthenium Sensitzer and Polymer Gel Electrolyte. *Nat. Mater.* **2003**, *2*, 402–407.
8. Mueggenburg, K. E.; Lin, X.-M.; Goldsmith, R. H.; Jaeger, H. M. Elastic Membranes of Close-Packed Nanoparticle Arrays. *Nat. Mater.* **2007**, *6*, 658–660.
9. Liu, G. L.; Yin, Y. D.; Kunchakarra, S.; Mukherjee, B.; Gerion, D.; Jett, S. D.; Bear, D. G.; Gray, J. W.; Alivisatos, A. P.; Lee, L. P. A Nanoplasmonic Molecular Ruler for Measuring Nuclease Activity and DNA Footprinting. *Nat. Nanotechnol.* **2006**, *1*, 47–52.
10. Bertorelle, F.; Wilhelm, C.; Roger, J.; Gazeau, F.; Menager, C.; Cabuil, V. Fluorescence-Modified Superparamagnetic Nanoparticles: Intracellular Uptake and Use in Cellular Imaging. *Langmuir* **2006**, *22*, 5385–5391.
11. Biggs, S.; Scales, P. J.; Leong, Y. K.; Healy, T. W. Effects of Citrate Adsorption on the Interactions between Zirconia Surfaces. *J. Chem. Soc., Faraday Trans.* **1995**, *91*, 2921–2928.
12. Sehgal, A.; Lalatonne, Y.; Berret, J. F.; Morvan, M. Precipitation-Redispersion of Cerium Oxide Nanoparticles with Poly(Acrylic Acid): Toward Stable Dispersions. *Langmuir* **2005**, *21*, 9359–9364.
13. Desset, S.; Spalla, O.; Cabane, B. Redispersion of Alumina Particles in Water. *Langmuir* **2000**, *16*, 10495–10508.

14. Desset, S.; Spalla, O.; Lixon, P.; Cabanet, B. From Powders to Dispersions in Water: Effect of Adsorbed Molecules on the Redispersion of Alumina Particles. *Langmuir* **2001**, *17*, 6408–6418.
15. Studart, A. R.; Amstad, E.; Gauckler, L. J. Colloidal Stabilization of Nanoparticles in Concentrated Suspensions. *Langmuir* **2007**, *23*, 1081–1090.
16. Traina, C. A.; Schwartz, J. Surface Modification Of Y_2O_3 Nanoparticles. *Langmuir* **2007**, *23*, 9158–9161.
17. Kuchibhatla, S.; Karakoti, A. S.; Seal, S. Hierarchical Assembly of Inorganic Nanostructure Building Blocks to Octahedral Superstructures - A True Template-Free Self-Assembly. *Nanotechnology* **2007**, *18*, 75303–75307.
18. Zhang, D. S.; Fu, H. X.; Shi, L. Y.; Pan, C. S.; Li, Q.; Chu, Y. L.; Yu, W. J. Synthesis of CeO_2 Nanorods via Ultrasonication Assisted by Polyethylene Glycol. *Inorg. Chem.* **2007**, *46*, 2446–2451.
19. Gawalt, E. S.; Avaltroni, M. J.; Danahy, M. P.; Silverman, B. M.; Hanson, E. L.; Midwood, K. S.; Schwarzbauer, J. E.; Schwartz, J. Bonding Organics To Ti Alloys: Facilitating Human Osteoblast Attachment and Spreading on Surgical Implant Materials. *Langmuir* **2003**, *19*, 200–204.
20. Dalsin, J. L.; Lin, L. J.; Tosatti, S.; Voros, J.; Textor, M.; Messersmith, P. B. Protein Resistance of Titanium Oxide Surfaces Modified by Biologically Inspired Mpeg-DOPA. *Langmuir* **2005**, *21*, 640–646.
21. Dobrovolskaia, M. A.; Mcneil, S. E. Immunological Properties of Engineered Nanomaterials. *Nat. Nanotechnol.* **2007**, *2*, 469–478.
22. Yu, T. Z.; Su, W. M.; Li, W. L.; Hua, R. N.; Chu, B.; Li, B. Ultraviolet Electroluminescence from Organic Light-Emitting Diode with Cerium(III)-Crown Ether Complex. *Solid-State Electron.* **2007**, *51*, 894–899.
23. Hung, I. M.; Wang, H. P.; Lai, W. H.; Fung, K. Z.; Hon, M. H. Preparation of Mesoporous Cerium Oxide Templated by Tri-Block Copolymer for Solid Oxide Fuel Cell. *Electrochim. Acta* **2004**, *50*, 745–748.
24. Patsalas, P.; Logothetidis, S.; Metaxa, C. Optical Performance of Nanocrystalline Transparent Ceria Films. *Appl. Phys. Lett.* **2002**, *81*, 466–468.
25. Feng, X. D.; Sayle, D. C.; Wang, Z. L.; Paras, M. S.; Santora, B.; Sutorik, A. C.; Sayle, T. X. T.; Yang, Y.; Ding, Y.; Wang, X. D. Converting Ceria Polyhedral Nanoparticles into Single-Crystal Nanospheres. *Science* **2006**, *312*, 1504–1508.
26. Suphantharida, P.; Osseo-Asare, K. Cerium Oxide Slurries In CMP. Electrophoretic Mobility and Adsorption Investigations of Ceria/Silicate Interaction. *J. Electrochem. Soc.* **2004**, *151*, G658−G662.
27. Tarnuzzer, R. W.; Colon, J.; Patil, S.; Seal, S. Vacancy Engineered Ceria Nanostructures for Protection from Radiation-Induced Cellular Damage. *Nano Lett.* **2005**, *5*, 2573–2577.
28. Chen, J. P.; Patil, S.; Seal, S.; Mcginnis, J. F. Rare Earth Nanoparticles Prevent Retinal Degeneration Induced by Intracellular Peroxides. *Nat. Nanotechnol.* **2006**, *1*, 142–150.
29. Schubert, D.; Dargusch, R.; Raitano, J.; Chan, S. W. Cerium and Yttrium Oxide Nanoparticles are Neuroprotective. *Biochem. Biophys. Res. Commun.* **2006**, *342*, 86–91.
30. Nabavi, M. O. S. A. B. C.Surface Chemistry of Nanometric Ceria Particles in Aqueous Dispersions. *J. Colloid Interface Sci.* **1993**, *160*, 459–471.
31. Berret, J. F. Stoichiometry of Electrostatic Complexes Determined by Light Scattering. *Macromolecules* **2007**, *40*, 4260–4266.
32. Spalla, O.; Cabane, B. Growth of Colloidal Aggregates through Polymer Bridging. *Colloid Polym. Sci.* **1993**, *271*, 357–371.
33. Studart, A. R.; Amstad, E.; Antoni, M.; Gauckler, L. J. Rheology of Concentrated Suspensions Containing Weakly Attractive Nanoparticles. *J. Am. Ceram. Soc.* **2006**, *89*, 2418–2425.
34. Lyklema, J., *Fundamentals of Interface And Colloid Science;* Academic Press: London, 1991; Vol. 1.
35. Ulrich, S.; Laguecir, A.; Stoll, S. Complexation of a Weak Polyelectrolyte with a Charged Nanoparticle. Solution Properties and Polyelectrolyte Stiffness Influences. *Macromolecules* **2005**, *38*, 8939–8949.
36. Ulrich, S.; Laguecir, A.; Stoll, S. Complex Formation between a Nanoparticle and a Weak Polyelectrolyte Chain: Monte Carlo Simulations. *J. Nanoparticle Res.* **2004**, *6*, 595–603.
37. Gao, W.; Dickinson, L.; Grozinger, C.; Morin, F. G.; Reven, L. Self-Assembled Monolayers of Alkylphosphonic Acids on Metal Oxides. *Langmuir* **1996**, *12*, 6429–6435.
38. Wang, J. B.; Lee, H. K.; Huang, T. J. Synergistic Catalysis of Carbon Dioxide Hydrogenation into Methanol by Yttria-Doped Ceria/Gamma-Alumina-Supported Copper Oxide Catalysts: Effect of Support and Dopant. *Catal. Lett.* **2002**, *83*, 79–86.
39. Chane-Ching, J.-Y. Preparing A Dispersible, Sol-Forming Cerium (IV) Composition. U.S. Patent 5308548 A 1994.
40. Chen, H. I.; Chang, H. Y. Synthesis of Nanocrystalline Cerium Oxide Particles by The Precipitation Method. *Ceram. Int.* **2005**, *31*, 795–802.
41. Berret, J. F.; Sehgal, A.; Morvan, M.; Sandre, O.; Vacher, A.; Airiau, M. Stable Oxide Nanoparticle Clusters Obtained by Complexation. *J. Colloid Interface Sci.* **2006**, *303*, 315–318.
42. Fleer, G. J.; Cohen Stuart, M. A.; Scheutjens, J. M. H. M.; Cosgrove, T.; Vincent, B. *Polymers at Interfaces*; Chapman & Hall: London, 1993; 66–76.
43. Dijt, J. C.; Stuart, M. A. C.; Fleer, G. J. Reflectometry as A Tool for Adsorption Studies . *Adv. Colloid Interface Sci.* **1994**, *507*, 9–101.
44. Gage, R. A.; Currie, E. P. K.; Cohen Stuart, M. A. Adsorption of Nanocolloidal SiO_2 Particles on PEO Brushes. *Macromolecules* **2001**, *34*, 5078–5080.
45. Burgh, S. V. D.; Fokkink, R.; Keizer, A. D.; Stuart, M. A. C. Complex Coacervation Core Micelles as Anti-Fouling Agents on Silica and Polystyrene Surfaces. *Colloids Surf. A* **2004**, *242*, 167–174.
46. Iruthayaraj, J.; Poptoshev, E.; Vareikis, A.; Makuska, R.; Wal, A. V. D.; Claesson, P. M. Adsorption of Low Charge Density Polyelectrolyte Containing Poly(ethylene oxide) Side Chains on Silica: Effects of Ionic Strength and pH. *Macromolecules* **2005**, *38*, 6152–6160.
47. Naderi, A.; Claesson, P. M. Adsorption Properties of Polyelectrolyte-Surfactant Complexes on Hydrophobic Surfaces Studied by QCM-D. *Langmuir* **2006**, *22*, 7639–7645.
48. Koutsopoulos, S.; Patzsch, K.; Bosker, W. T. E.; Norde, W. Adsorption of Trypsin on Hydrophilic and Hydrophobic Surfaces. *Langmuir* **2007**, *23*, 2000–2006.
49. Qi, L.; Chapel, J.-P.; Castaing, J.-P.; Fresnais, J.; Berret, J.-F. Stability and Adsorption Properties of Electrostatic Complexes: Design of Hybrid Nanostructures for Coating Applications. *Langmuir* **2007**, *23*, 11996–11998.